ChemComm

Accepted Manuscript

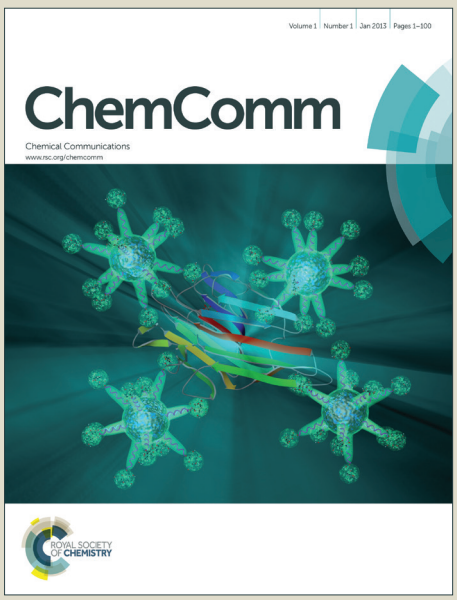

ROYAL SOCIETY OF CHEMISTRY

www.rsc.org/chemcomm

Journal Name

RSCPublishing

COMMUNICATION

Towards covalent organic frameworks with predesignable and aligned open docking sites

Cite this: DOI: 10.1039/x0xx00000x

Xiong Chen,[a] Ning Huang,[a] Jia Gao,[a] Hong Xu,[a] Fei Xu[a] and Donglin Jiang[a]

Received 00th January 2012,
Accepted 00th January 2012

DOI: 10.1039/x0xx00000x

www.rsc.org/

A strategy for the synthesis of covalent organic frameworks with open docking sites is developed. The docking sites are ordered on the channel walls and structurally predesignable for meeting various types of noncovalent interactions, thus opening a way towards designing supramolecular materials based on crystalline porous organic frameworks.

Covalent organic frameworks (COFs) are a class of crystalline porous polymers with atomically precise and predictable network of building blocks in two-dimensional (2D) or three-dimensional (3D) topology.[1] Compared with other crystalline porous materials, COFs are unique in that they are made from lightweight elements linked by covalent linkages. A distinct feature is that COFs allow a total control over structures, including skeleton and pore size and shape. In particular, 2D COFs integrate organic building blocks into covalent 2D sheets and layered frameworks, which constitute periodic π columnar arrays and directional open nanochannels. 2D COFs have emerged as a powerful platform for designing functional polymers with luminescence,[2] photoconduction,[2,3] sensing,[2b] catalysis,[4] charge transport[3a,3b,5] and separation[6] and photovoltaic[7] properties.

From a synthetic perspective, COFs are attractive motifs for incorporation of open docking sites into ordered alignment, which constitute a new class of COFs for supramolecular architecture. However, COFs with open docking sites remain a synthetic challenge. Here we report a strategy for the construction of 2D COFs with open docking sites in the skeletons. We highlight that the docking sites are ordered on the channel walls and are structurally designable for meeting various types of noncovalent interactions.

Our strategy for embedding open docking sites is targeted on the walls of one-dimensional (1D) channels of 2D COFs; this configuration allows an easy access of guest molecules through the 1D channels to the docking sites for supramolecular construction. Both the vertices and edges of 2D COFs can be explored for anchoring open docking sites, whereas the vertices are usually highly substituted for the skeleton development of COFs and positions available for further appending docking sites are thus limited. In contrast, the edge units have more free positions for functionalization. Based on this structural feature, we explored the edge units of COFs for loading open docking sites. We demonstrated the concept by using imine-linked COFs as a scaffold, to which four kinds of edge units with different functionalities were introduced. We synthesized 4,4',4",4'"-(pyrene-1,3,6,8-tetrayl) tetraaniline (PyTTA) bearing four amino groups as the vertices and developed four different aldehydes as the edge units, including 2,5-dihydroxyterephthalaldehyde (DHTA), 2,3-dihydroxy terephthalaldehyde (2,3-DHTA), [2,2'-bipyridine]-5,5'-dicarbaldehyde (2,2'-BPyDCA) and [3,3'-bipyridine]-6,6'-dicarbaldehyde (3,3'-BPyDCA), whereas –OH, $-(OH)_2$ and 2,2'- and 3,3'-bipyridine docking sites were embedded in the channel walls. The –OH and pyridine groups are well-established for various supramolecular constructions. Condensation of PyTTA and aldehydes in mixture solvents in the presence of acetic acid catalyst under 120 ºC afforded the Py-DHPh COF, Py-2,3-DHPh COF, Py-2,2'-BPyPh COF and Py-3,3'-BPyPh COF in good isolated yields (Scheme 1, ESI†).

We optimized the solvothermal conditions, including solvents and reaction times, for the synthesis of highly crystalline COFs (ESI†). Fig. S1 summarized the X-ray diffraction (XRD) results. The COFs exhibited characteristic C=N vibration stretches for imines at 1608-1622 cm^{-1} (Fig. S2, Table S1, ESI†). Elemental analysis confirmed that the C, H and N contents of the COFs were close to the calculated values expected for an infinite 2D sheet (Table S2, ESI†). Field-emission scanning electron microscopy images revealed belt or flake-like morphologies (Fig. S3, ESI†). Thermal gravimetric analysis suggested that the COFs are stable up to 400 ºC (Fig. S4, ESI†).

These COFs are highly crystalline materials with strong XRD signals (Fig. 1). The Py-DHPh COF exhibited diffraction peaks at 3.68º, 5.28º, 7.28°, 8.56°, 11.28°, 15.38º and 23.76º, which are assignable to the (110), (020), (220), (030), (040), (060) and (001) facets,

[a]Department of Materials Molecular Science, Institute for Molecular Science, National Institutes of Natural Sciences, 5-1 Higashiyama, Myodaiji, Okazaki 444-8787, Japan; E-mail: jiang@ims.ac.jp

†Electronic Supplementary Information (ESI) available: Methods, XRD data, structural simulation, FT-IR and electronic absorption spectra, TGA, SEM and gas adsorption analysis. See DOI: 10.1039/b000000x/

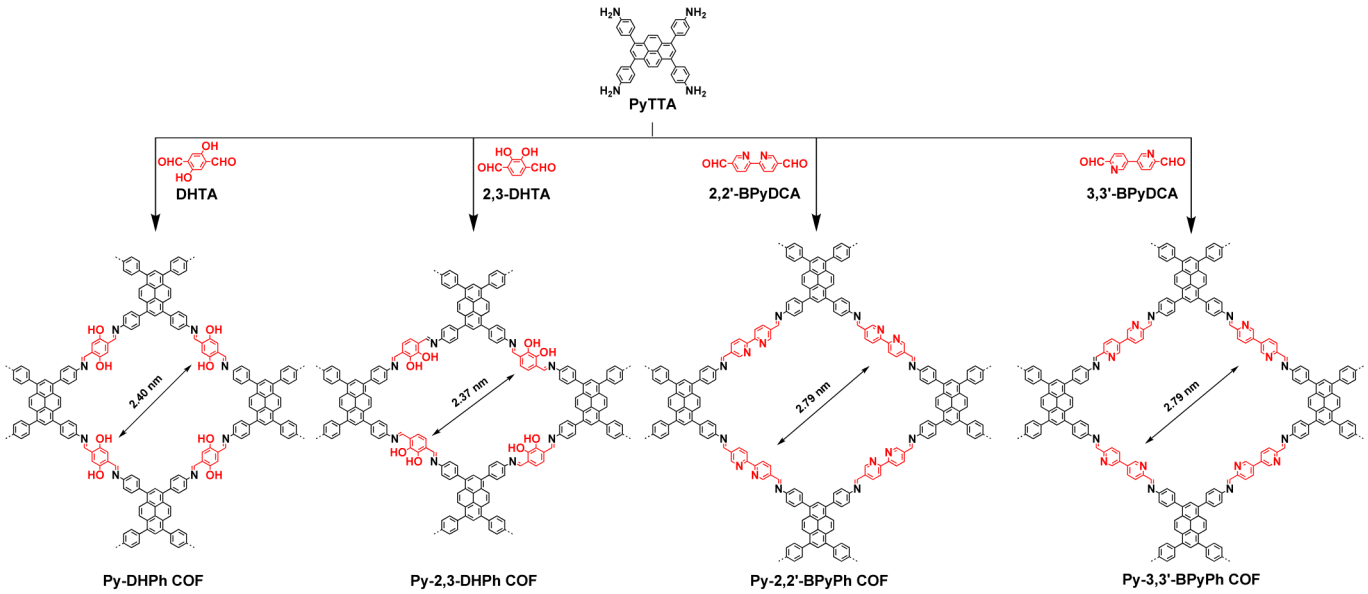

Scheme 1 Schematic representation of the imine-linked pyrene COFs with predesigned and aligned open docking sites (phenol and pyridine units in red).

respectively (Fig. 1A). The Py-2,3-DHPh COF demonstrated XRD peaks at 3.72°, 5.50°, 7.54°, 8.72°, 11.40°, 12.22°, 15.32° and 23.98°, which are attributed to the (110), (020), (220), (030), (040), (240), (440) and (001) facets, respectively (Fig. 1B). The Py-2,2'-BPyPh COF displayed main diffractions at 3.16°, 4.58°, 6.38°, 9.74°, 12.98° and 23.86°, which can be assigned to the (110), (020), (220), (330), (440), and (001) facets, respectively (Fig. 1C). The Py-3,3'-BPyPh COF showed main peaks at 3.16°, 4.80°, 6.38°, 7.44°, 9.64°, 12.92° and 23.54°, which can be attributed to (110), (020), (220), (030), (330), (240) and (001) facets, respectively (Fig. 1D). The presence of (001) facets indicates that these 2D COFs have periodic orders in all three dimensions. Pawley refinements (Fig. S5A, D, G, J, green curves, ESI†) confirmed the above peak assignments as evidenced by their negligible differences (black curves).

XRD pattern simulation by using AA-stacking mode reproduced the XRD signal position and peak intensity (Fig. S5A, D, G, J, blue curves, ESI†). This layer structure results in open 1D channels (Fig. S5B, E, H, K, ESI†). In sharp contrast, staggered AB stacking mode with offset by *a*/2 and *b*/2 gave XRD patterns (purple curves) that could not reproduce the experimental XRD patterns. In this case, the pores are overlapped by neighboring sheets (Fig. S5C, F, I, L, ESI†). In the case of AA-stacking mode, the *a*, *b*, *c* values for Py-DHPh COF are *a* = 35.82 Å, *b* = 31.90 Å, *c* = 4.69 Å; for Py-2,3-DHPh COF are *a* = 36.15 Å, *b* = 31.30 Å, *c* = 3.60 Å; for Py-2,2'-BPyPh COF are *a* = 42.14 Å, *b* = 36.90 Å, *c* = 4.33 Å and for Py-3,3'-BPyPh COF are *a* = 40.55 Å, *b* = 39.08 Å, *c* = 3.60 Å, respectively (Table S3, ESI†).

To investigate whether the 1D channels of the COFs are accessible and their porosity, nitrogen sorption isotherm measurements at 77 K were conducted. These COFs exhibited reversible type IV sorption curves (Fig. 2A-D),[9] which are characteristics of mesoporous materials. The Brunauer-Emmett-Teller (BET) surface areas were calculated to be as high as 1895, 1932, 2349 and 2200 $m^2 g^{-1}$ for the Py-DHPh COF, Py-2,3-DHPh COF, Py-2,2'-BPyPh COF and Py-3,3'-BPyPh COF, respectively. These surface areas are among the highest values for the imine-linked COFs reported based on

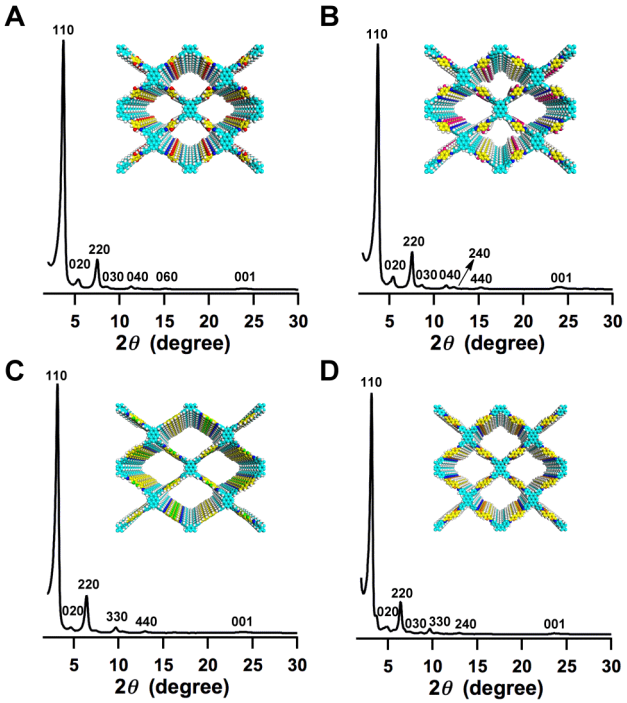

Fig. 1 XRD patterns of (A) Py-DHPh COF, (B) Py-2,3-DHPh COF, (C) Py-2,2'-BPyPh COF and (D) Py-3,3'-BPyPh COF. Insets are the graphic view of a 2 × 2 porous framework in the AA-stacking mode.

N_2 sorption; in particular, the Py-2,2'-BPyPh COF exceeds all other imine-linked COFs.[4,5a,8] The total pore volumes were estimated to be 1.45, 1.51, 1.85 and 1.49 $cm^3 g^{-1}$ for the Py-DHPh COF, Py-2,3-DHPh COF, Py-2,2'-BPyPh COF and Py-3,3'-BPyPh COF, respectively (Table S4, ESI†).We evaluated the pore size distributions by using the nonlocal density function theory (NLDFT) method. The COFs have one main peak centered at 1.99, 1.95, 2.45, and 2.52 nm, which are close to their theoretical values (Fig. S6, ESI†). These results indicate that the docking sites on the channel walls are accessible to guest molecules for supramolecular constructions.

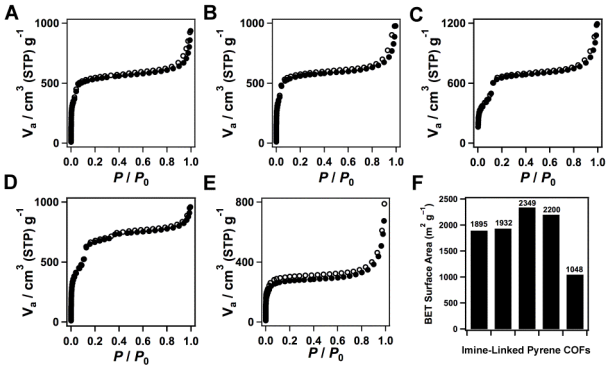

Fig. 2 Nitrogen sorption isotherms of (A) Py-DHPh COF, (B) Py-2,3-DHPh COF, (C) Py-2,2'-BPyPh COF, (D) Py-3,3'-BPyPh COF and (E) VO@Py-2,3-DHPh COF measured at 77 K. (F) BET surface areas of the COFs (from left to right, the bar coresponds to the Py-DHPh COF, Py-2,3-DHPh COF, Py-2,2'-BPyPh COF, Py-3,3'-BPyPh COF and VO@Py-2,3DHPh COF).

Imine linkage constitutes one type of conjugation bonds, how the docking sites affect the π conjugation of COFs and thus their π electronic properties is an interesting point to be elucidated. We conducted solid-state absorption spectroscopy to evaluate the absorption bands of COFs. The Py-DHPh COF, Py-2,3-DHPh COF, Py-2,2'-BPyPh COF, and Py-3,3'-BPyPh COF exhibited absorption bands at 469, 458, 442 and 445 nm, respectively (Fig. S7), which were 53, 42, 26 and 29-nm redshifts in comparison with the PyTTA monomer (416 nm). These results indicate that an extended π conjugation over the 2D sheet of the COFs. The difference in the redshift suggests that the edge units with different docking sites can perturb the conjugation status. The docking sites with phenol groups prefer a planar sheet conformation that promotes π conjugation, whereas the docking sites with bipyridine units cause a twisted conformation of the 2D sheets and trigger pyridine nitrogen induced p-π overlap that localizes the π clouds.

To demonstrate the potential of these crystalline COFs as a scaffold for the supramolecular construction, we conducted additional experiments. We chose the Py-2,3-DHPh COF as a scaffold and metallated the catechol groups with vanadium(IV)-oxy acetylacetonate [$VO(acac)_2$] (Scheme 2, ESI†). Treatment of the Py-2,3-DHPh COF sample having a BET surface area of 1432 m^2 g^{-1} with $VO(acac)_2$ in THF at 50 °C for 24 h caused a clear color change from red to black and yielded quantitative isolation of VO@Py-2,3-DHPh COF. The resulting VO@Py-2,3-DHPh COF consists of V=O groups on the channel walls with an almost quantitative conversion (0.96 V=O/catechol in molar ratio), as determined by inductively coupled plasma atomic emission spectroscopy analysis (ESI†). The XRD patterns (Fig. S8A, ESI†) confirmed that the crystallinity was maintened in the VO@Py-2,3-DHPh COF. The N_2 sorption curves (Fig. 2E) revealed microporous characteristics, whereas the BET surface area was evaluated to be 1048 m^2 g^{-1} (Fig. 2F). The pore volume was evaluated to be 1.16 cm^3 g^{-1} (Fig. S8B, ESI†). The VO@Py-2,3-DHPh COF consists of only one kind of micropore with size of 1.82 nm (Fig. S8B, ESI†). Interestingly, the absorption band was broadened to longer wavelength with the peak maximum red-shifted from 458 to 468 nm (Fig. S8C, D, ESI†). This is caused by the coordination of V=O to the edge units of the COFs. The VO@ Py-2,3-DHPh COF samples are stable in various solvents and are thermally stable up to 300 °C (Figure S9, ESI). Because V=O sites are well-established catalytic centers,[10] the VO@Py-2,3-DHPh COF with dense V=O units confined within the open channels constitutes an intriguing heterogeneous catalytic system worthy of further investigation.

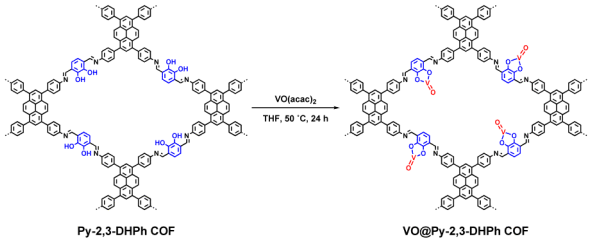

Scheme 2 Synthesis of the VO@Py-2,3-DHPh COF.

In summary, we have developed a general strategy for construction of a new class of COFs that offer open docking sites on the channel walls. These COFs feature ordered alignment of binding sites and predesignable skeletons. Metallation converts the open frameworks into supramolecular COFs with dense and aligned catalytic V=O sites confined within the nanochannels. These remarkable results open a way to supramolecular architecture based on crystalline open structures of COFs.

This work was supported by a Grant-in-Aid for Scientific Research (A) (24245030) from MEXT, Japan.

Notes and references

1 X. Feng, X. Ding, D. Jiang, *Chem. Soc. Rev.*, 2012, **41**, 6010-6022.
2 (a) S. Wan, J. Guo, J. Kim, H. Ihee, D. Jiang, *Angew. Chem. Int. Ed.*, 2008, **47**, 8826-8830; (b) S. Dalapati, S. Jin, J. Gao, Y. Xu, A. Nagai, D. Jiang, *J. Am. Chem. Soc.*, 2013, **135**, 17310-17313.
3 (a) X. Feng, L. Liu, Y. Honsho, A. Saeki, S. Seki, S. Irle, Y. P. Dong, A. Nagai, D. Jiang, *Angew. Chem., Int. Ed.*, 2012, **51**, 2618-2622; (b) M. Dogru, M. Handloser, F. Auras, T. Kunz, D. Medina, A. Hartschuh, P. Knochei, T. Bein, *Angew. Chem., Int. Ed.*, 2013, **52**, 2920-2924.
4 (a) S. Y. Ding, J. Gao, Q. Wang, Y. Zhang, W. G. Song, C. Y. Su, W. Wang, *J. Am. Chem. Soc.*, 2011, **133**, 19816-19822; (b) H. Xu, X. Chen, J. Gao, J. Lin, M. Addicoat, S. Irle, D. Jiang. *Chem. Commun.*, 2014, **47**, 1292-1294.
5 (a) S. Wan, F. Gndara, A. Asano, H. Furukawa, A. Saeki, S. K. Dey, L. Liao, M. W. Ambrogio, Y. Y. Botros, X. Duan, S. Seki, J. F. Stoddart, O. M. Yaghi, *Chem. Mater.*, 2011, **23**, 4094-4097; (b) X. Feng, L. Chen, Y. Honsho, O. Saengsawang, L. Liu, L. Wang, A. Saeki, S. Irle, S. Seki, Y. Dong, D. Jiang, *Adv. Mater.*, 2012, **24**, 3026-3031.
6 S. Jin, X. Ding, X. Feng, M. Supur, K. Furukawa, S. Takahashi, M. Addicoat, M. E. El-Khouly, T. Nakamura, S. Irle, S. Fukuzumi, A. Nagai, D. Jiang, *Angew. Chem., Int. Ed.*, 2013, **52**, 2017-2021.
7 J. Guo, Y. Xu, S. Jin, L. Chen, T. Kaji, Y. Honsho, M. Addicoat, J. Kim, A. Saeki, H. Ihee, S. Seki, S. Irle, M. Hiramoto, J. Gao, D. Jiang, *Nat. Commun.*, 2013, **4**:2736, doi:10.1038/ncomms3736.
8 (a) F. J. Uribe-Romo, J. R. Hunt, H. Furukawa, C. KlÖck, M. O'Keeffe, O. M. Yaghi. *J. Am. Chem. Soc.*, 2009, **131**, 4570-4571; (b) X. Chen, M. Addicoat, S. Irle, A. Nagai, D. Jiang, *J. Am. Chem. Soc.*, 2013, **135**, 546-549; (c) S. Kandambeth, D. B. Shinde, M. K. Panda, B. Lukose, T. Heine, R. Banerjee, *Angew. Chem., Int. Ed.*, 2013, **52**, 13052-13056; (d) M. G. Rabbani, A. K. Sekizkardes, Z. Kahveci, T. E. Reich, R. Ding, H. M. El-Kaderi. *Chem. Eur. J.*, 2013, **19**, 3324-3328; (e) Y. Zhang, J. Su, H. Furukawa, Y. Yun, F. Gándara, A. Duong, X. Zou, O. M. Yaghi, *J. Am. Chem. Soc.*, 2013, **135**, 16336-16339; (f) W. Huang, Y. Jiang, X. Li, X. Li, J. Wang, Q. Wu, X. Liu, *ACS Appl. Mater. Interfaces*, 2013, **5**, 8845-8849; (g) D. N. Bunck, W. R. Dichtel, *Chem. Commun.*, 2013, **49**, 2457-2459; (h) P. Kuhn, M. Antonietti, A. Thomas, *Angew. Chem. Int. Ed.*, 2008, **47**, 3450-3453.
9 K. M. Sing, D. H. Everett, R. A. W. Haul, L. Moscou, R. A. Pierotti, J. Rouquerol, T. Siemieniewska, *Pure & Appl. Chem.*, 1985, **57**, 603-619.
10 K. Nomura, S. Zhang, *Chem. Rev.*, 2011, **111**, 2342-2362.